Appl. Math. Mech. -Engl. Ed., **43**(4), 479–496 (2022)

APPLIED MATHEMATICS AND MECHANICS (ENGLISH EDITION)

https://doi.org/10.1007/s10483-022-2839-6

Natural dynamic characteristics of a circular cylindrical Timoshenko tube made of three-directional functionally graded material*

Ye TANG[1,2], Jiye XU[1], Tianzhi YANG[3,†]

1. School of Mechanical Engineering, Anhui Polytechnic University, Wuhu 241000, Anhui Province, China;
2. Department of Mechanics, Tianjin University, Tianjin 300350, China;
3. School of Mechanical Engineering and Automation, Northeastern University, Shenyang 110819, China

(Received Dec. 13, 2021 / Revised Jan. 28, 2022)

Abstract The natural dynamic characteristics of a circular cylindrical tube made of three-directional (3D) functional graded material (FGM) based on the Timoshenko beam theory are investigated. Hamilton's principle is utilized to derive the novel motion equations of the tube, considering the interactions among the longitudinal, transverse, and rotation deformations. By dint of the differential quadrature method (DQM), the governing equations are discretized to conduct the analysis of natural dynamic characteristics. The Ritz method, in conjunction with the finite element method (FEM), is introduced to verify the present results. It is found that the asymmetric modes in the tube are controlled by the 3D FGM, which exhibit more complicated shapes compared with the unidirectional (1D) and bi-directional (2D) FGM cases. Numerical examples illustrate the effects of the axial, radial, and circumferential FGM indexes as well as the supported edges on the natural dynamic characteristics in detail. It is notable that the obtained results are beneficial for accurate design of smart structures composed from multi-directional FGM.

Key words circular cylindrical tube, three-directional (3D) functionally graded material (FGM), asymmetric mode, natural dynamic characteristic, differential quadrature method (DQM)

Chinese Library Classification O343.6
2010 Mathematics Subject Classification 74F05

1 Introduction

Functionally graded material (FGM) is a class of advanced composite structures, which usually contains two or more constitutions with desired characteristics by designing the volume

* Citation: TANG, Y., XU, J. Y., and YANG, T. Z. Natural dynamic characteristics of a circular cylindrical Timoshenko tube made of three-directional functionally graded material. *Applied Mathematics and Mechanics* (*English Edition*), **43**(4), 479–496 (2022) https://doi.org/10.1007/s10483-022-2839-6

† Corresponding author, E-mail: yangtianzhi@me.neu.edu.cn

Project supported by the National Natural Science Foundation of China (Nos. 11902001 and 12072221), the China Postdoctoral Science Foundation (No. 2018M641643), and the Anhui Provincial Natural Science Foundation of China (Nos. 1908085QA13 and 1808085ME128)

fraction of the body according to a certain mixture rule. Due to the continuous and smooth variation in the graded element, there are some outstanding features including high resistance, lightweight, and flexibility[1–3]. Consequently, the superior composites have a wide range of applications under hash working conditions, e.g., the plasma surface of fusion reactor and spacecraft heat shield. It is not surprising that FGM structures, e.g., FGM beam[4], FGM plate[5], FGM shell[6], and FGM pipe[7–8], are developed as perfect candidates to construct the main element in the machine construction.

Another famous structure applied in a great number of engineering fields, e.g., aerospace, civil, mechanical, and naval engineering, is hollow cylinder, which is selected as the necessary unit from micro to macro scales, e.g., microtubule, carbon nanotube, and fuel tank[9–10]. Hollow cylinder in service often withstands severe complex loads, which directly affects the structural stability, reliability, and integrity. In order to optimize the tube responses for improving mechanical behaviors, FGM has been utilized to construct hollow circular cylinders. The dynamic characteristics and mechanics of FGM hollow cylinders are of interesting topics, and have received vast attention. By virtue of the semi-analytical finite element method (FEM), Kadoli and Ganesan[11] investigated the buckling and vibration of FGM cylinders with the action of thermal stresses. By dint of a two-step perturbation technique, Fu et al.[12] investigated the thermal buckling and postbulking problems of FGM tubes with material properties varying graded along the radial direction according to the power-law function. With the help of a refined higher-order beam and the modified couple stress theories, Lu et al.[13–14] used a functionally graded (FG) graphene platelet reinforced composite (GPLRC) multilayer to construct microtubes, and studied the free vibration, stability, and postbuckling behaviors. Fuselages of aerospace crafts and shuttles[15] often endure super-high thermal loads in two or three orientations. Conventional unidirectional (1D) FGM can no longer satisfy the demand of several physical fields. To fulfill the increasing requirements of advanced materials undergoing multi-directional loads, multi-directional FGM is proposed so as to meet the design potential in more general physical fields, e.g., multi-directional severe variations of temperature.

In recent years, scholars have widely focused on multi-directional FGM, owing to its outstanding superiority over 1D FGM. In order to acquire effective applications of multi-directional FGM, several researchers have carried out investigations on the mechanical characteristics of bi-directional (2D) FGM, e.g., flexural response[16], bucking[17], vibration[18–19], postbucking[20], hygro-thermal behavior[21], and magneto-electro-elastic coupling mechanism[22–23]. However, the number of analyses on structures made of three-directional (3D) FGM is still limited. Hadi et al.[24] took the advantage of the differential quadrature technique to study the natural dynamic characteristics of 3D FGM nanobeams with the nonlocal strain gradient theory.

To the best of the authors' knowledge, most of previous works related to the static and dynamic characteristics of FGM circular cylindrical tubes address uni-directional FGM. The novelty of the present work is to use 3D FGM to construct circular cylindrical tubes for resisting multi-directional loads. It has been shown from our previous investigations that 2D FGM may induce asymmetric modes in free vibration, which significantly affects the structural behavior. It is confirmed that 3D FGM tubes exhibit different dynamic characteristics over conventional FGM tubes. In this paper, the dynamic characteristics of a circular cylindrical Timoshenko tube made of 3D FGM under general boundary conditions are investigated by means of the differential quadrature method (DQM), the Ritz method, and the FEM. In Section 2, the relative theory and formulation are introduced. In Section 3, the solution procedure is described. The numerical results are presented in Section 4. The main conclusions are summarized in Section 5.

2 Theory and formulation

As seen in Fig. 1, we present a circular cylindrical Timoshenko tube made of 3D FGM, in which L is the length, R_{i} is the inner radius, and R_{o} is the outer radius. In the tube system,

we define two types of coordinate systems, i.e., the Cartesian coordinates (x, y, z) and the cylindrical coordinates (θ, r, x). It is noted that the relationship between the two coordinate systems is $r^2 = z^2 + y^2$, $y = r\cos\theta$, and $z = r\sin\theta$. We assume that the 3D FGM Timoshenko tube has a continuous and smooth property varying along the axial, radial, and circumferential orientations, so that the elastic modulus $\widetilde{E}(x, r, \theta)$, the density $\widetilde{\rho}(x, r, \theta)$, and Poisson's ratio $\widetilde{\nu}(x, r, \theta)$ are

$$\widetilde{E}(x,r,\theta) = \Theta_1(x)\Big(E^{\mathrm{c}}\Big(\frac{r-R_{\mathrm{i}}}{R_{\mathrm{o}}-R_{\mathrm{i}}}\Big)^n\Big(\frac{\theta}{2\pi}\Big)^k + E^{\mathrm{m}}\Big(1-\Big(\frac{r-R_{\mathrm{i}}}{R_{\mathrm{o}}-R_{\mathrm{i}}}\Big)^n\Big(\frac{\theta}{2\pi}\Big)^k\Big)\Big), \tag{1}$$

$$\widetilde{\rho}(x,r,\theta) = \Theta_2(x)\Big(\rho^{\mathrm{c}}\Big(\frac{r-R_{\mathrm{i}}}{R_{\mathrm{o}}-R_{\mathrm{i}}}\Big)^n\Big(\frac{\theta}{2\pi}\Big)^k + \rho^{\mathrm{m}}\Big(1-\Big(\frac{r-R_{\mathrm{i}}}{R_{\mathrm{o}}-R_{\mathrm{i}}}\Big)^n\Big(\frac{\theta}{2\pi}\Big)^k\Big)\Big), \tag{2}$$

$$\widetilde{\nu}(x,r,\theta) = \Theta_3(x)\Big(\nu^{\mathrm{c}}\Big(\frac{r-R_{\mathrm{i}}}{R_{\mathrm{o}}-R_{\mathrm{i}}}\Big)^n\Big(\frac{\theta}{2\pi}\Big)^k + \nu^{\mathrm{m}}\Big(1-\Big(\frac{r-R_{\mathrm{i}}}{R_{\mathrm{o}}-R_{\mathrm{i}}}\Big)^n\Big(\frac{\theta}{2\pi}\Big)^k\Big)\Big), \tag{3}$$

where $\Theta_1(x)$, $\Theta_2(x)$, and $\Theta_3(x)$ are arbitrary functions. n and k denote the radial and circumferential FGM indexes, respectively, which are relevant to the volume fraction varied along the radial and circumferential orientations. The superscripts c and m represent the corresponding properties of pure ceramic and metal, respectively.

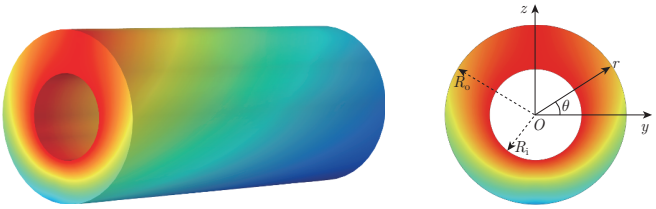

(a) Main view (b) Cross-section view

Fig. 1 Schematic diagram of a circular cylindrical Timoshenko tube made of 3D FGM (color online)

According to the Timoshenko beam theory, the displacement fields $(\widetilde{u}_1, \widetilde{u}_2, \widetilde{u}_3)$ of the 3D FGM tube are introduced as follows:

$$\widetilde{u}_1 = u_0(x,t) + z\psi_{\mathrm{c}}(x,t), \quad \widetilde{u}_2 = 0, \quad \widetilde{u}_3 = w_{\mathrm{h}}(x,t), \tag{4}$$

where u_0 and w_{h} represent the axial and transverse deflections of any point in the 3D FGM tube on the x-axis, and ψ_{c} denotes the rotation of the tube cross-section. Introduce the strain-displacement relationship as follows:

$$\widetilde{\varepsilon}_{xx} = \frac{\partial\widetilde{u}_1}{\partial x} = \frac{\partial u_0}{\partial x} + z\frac{\partial\psi_{\mathrm{c}}}{\partial x}, \quad \widetilde{\gamma}_{xz} = \frac{\partial\widetilde{u}_1}{\partial z} + \frac{\partial\widetilde{u}_3}{\partial x} = \frac{\partial w_{\mathrm{h}}}{\partial x} + \psi_{\mathrm{c}}. \tag{5}$$

According to Hooke's law and the assumption of small deformations, the stresses in the 3D FGM tube are

$$\widetilde{\sigma}_{xx} = \widetilde{E}\widetilde{\varepsilon}_{xx}, \quad \widetilde{\tau}_{xz} = \widetilde{k}_{\mathrm{s}}\widetilde{G}\widetilde{\gamma}_{xz}, \tag{6}$$

where $\widetilde{k}_{\mathrm{s}}$ denotes the shear correction factor, which is employed to account for the non-uniform shear stress distribution, and $\widetilde{G}$ is the shear modulus of the tube defined by $\widetilde{G} = \widetilde{E}/(2(1+\widetilde{\vartheta}))$. On the basis of Cartesian coordinates, the potential energy of the 3D FGM tube takes the following form:

$$\Pi_U = \frac{1}{2}\int_{\widehat{V}}(\widetilde{\sigma}_{xx}\widetilde{\varepsilon}_{xx} + \widetilde{\tau}_{xz}\widetilde{\gamma}_{xz})\mathrm{d}\widehat{V}, \tag{7}$$

where $\widehat{V}$ is the volume of the tube. Substituting Eqs. (5) and (6) into Eq. (7) yields

$$\begin{aligned}\Pi_U &= \frac{1}{2}\int_0^L \int_{\widehat{A}} \Big(\widetilde{\sigma}_{xx}\frac{\partial u_0}{\partial x} + \widetilde{\sigma}_{xx} z \frac{\partial \psi_{\mathrm{c}}}{\partial x} + \widetilde{\tau}_{xz}\Big(\frac{\partial w_{\mathrm{h}}}{\partial x} + \psi_{\mathrm{c}}\Big)\Big)\mathrm{d}\widehat{A}\mathrm{d}x \\ &= \frac{1}{2}\int_0^L \widetilde{N}_\Delta \frac{\partial u_0}{\partial x} + \widetilde{M}_\Delta \frac{\partial^2 w_{\mathrm{h}}}{\partial x^2} + \widetilde{Q}_\Delta\Big(\frac{\partial w_{\mathrm{h}}}{\partial x} + \psi_{\mathrm{c}}\Big)\mathrm{d}x, \end{aligned} \tag{8}$$

where $\widehat{A}$ is the cross-sectional area of the tube. The axial force $\widetilde{N}_\Delta$, the bending moment $\widetilde{M}_\Delta$, and the shear force $\widetilde{Q}_\Delta$ are defined by

$$(\widetilde{N}_\Delta, \widetilde{M}_\Delta, \widetilde{Q}_\Delta) = \int_{\widehat{A}} (\widetilde{\sigma}_{xx}, \widetilde{\sigma}_{xx} z, \widetilde{\tau}_{xz})\mathrm{d}\widehat{A}. \tag{9}$$

Substituting Eqs. (5)–(6) into Eq. (9) yields

$$\begin{cases} \widetilde{N}_\Delta = B^1_{xx}\Theta_1(x)\dfrac{\partial u_0}{\partial x} + B^2_{xx}\Theta_1(x)\dfrac{\partial \psi_{\mathrm{c}}}{\partial x}, \\ \widetilde{M}_\Delta = B^2_{xx}\Theta_1(x)\dfrac{\partial u_0}{\partial x} + B^3_{xx}\Theta_1(x)\dfrac{\partial \psi_{\mathrm{c}}}{\partial x}, \quad \widetilde{Q}_\Delta = \widetilde{k}_{\mathrm{s}} D_{55}\Big(\dfrac{\partial w_{\mathrm{h}}}{\partial x} + \psi_{\mathrm{c}}\Big), \end{cases} \tag{10}$$

in which

$$\begin{aligned}(B^1_{xx}, B^2_{xx}, B^3_{xx}) = \int_0^{2\pi}\int_{R_{\mathrm{i}}}^{R_{\mathrm{o}}} \Big(E^{\mathrm{c}}\Big(\frac{r-R_{\mathrm{i}}}{R_{\mathrm{o}}-R_{\mathrm{i}}}\Big)^n\Big(\frac{\theta}{2\pi}\Big)^k \\ + E^{\mathrm{m}}\Big(1-\Big(\frac{r-R_{\mathrm{i}}}{R_{\mathrm{o}}-R_{\mathrm{i}}}\Big)^n\Big(\frac{\theta}{2\pi}\Big)^k\Big)\Big)(1, r\sin\theta, r^2\sin^2\theta) r\mathrm{d}r\mathrm{d}\theta, \end{aligned} \tag{11}$$

$$D_{55}(x) = \int_0^{2\pi}\int_{R_{\mathrm{i}}}^{R_{\mathrm{o}}} \frac{\widetilde{E}}{2(1+\widetilde{\nu})} r\mathrm{d}r\mathrm{d}\theta. \tag{12}$$

The kinetic energy of the 3D FGM tube can be obtained as

$$\begin{aligned}\Pi_T &= \frac{1}{2}\int_{\widehat{V}} \widetilde{\rho}\Big(\Big(\frac{\partial \widetilde{u}_1}{\partial t}\Big)^2 + \Big(\frac{\partial \widetilde{u}_3}{\partial t}\Big)^2\Big)\mathrm{d}\widehat{V} \\ &= \frac{1}{2}\int_0^L \Theta_2(x)\Big(m_{br0}\Big(\frac{\partial u_0}{\partial t}\Big)^2 + 2m_{br1}\frac{\partial u_0}{\partial t}\frac{\partial \psi_{\mathrm{c}}}{\partial t} + m_{br2}\Big(\frac{\partial \psi_{\mathrm{c}}}{\partial t}\Big)^2 + m_{br0}\Big(\frac{\partial w_{\mathrm{h}}}{\partial t}\Big)^2\Big)\mathrm{d}x, \end{aligned} \tag{13}$$

where the inertia components m_{br0}, m_{br1}, and m_{br2} are

$$\begin{aligned}(m_{br0}, m_{br1}, m_{br2}) &= \int_{\widehat{A}} \frac{\widetilde{\rho}}{\Theta_2(x)}(1, z, z^2)\mathrm{d}A \\ &= \int_0^{2\pi}\int_{R_{\mathrm{i}}}^{R_{\mathrm{o}}} \Big(\rho^{\mathrm{c}}\Big(\frac{r-R_{\mathrm{i}}}{R_{\mathrm{o}}-R_{\mathrm{i}}}\Big)^n\Big(\frac{\theta}{2\pi}\Big)^k + \rho^{\mathrm{m}}\Big(1-\Big(\frac{r-R_{\mathrm{i}}}{R_{\mathrm{o}}-R_{\mathrm{i}}}\Big)^n\Big(\frac{\theta}{2\pi}\Big)^k\Big)\Big) \\ &\quad \cdot (1, r\sin\theta, r^2\sin^2\theta) r\mathrm{d}r\mathrm{d}\theta. \end{aligned} \tag{14}$$

Hamilton's principle is introduced as

$$\int_{t_1}^{t_2} (\delta\Pi_T - \delta\Pi_U)\mathrm{d}t = 0. \tag{15}$$

Substituting Eqs. (8) and (13) into Eq. (15) and then integrating by parts to the solutions yield the governing equations

$$\frac{\partial\Theta_1(x)\widetilde{N}_x}{\partial x} = \Theta_2(x)\Big(m_{br0}\frac{\partial^2 u_0}{\partial t^2} + m_{br1}\frac{\partial^2\psi_{\mathrm{c}}}{\partial t^2}\Big), \tag{16}$$

$$\frac{\partial\Theta_1(x)\widetilde{Q}_\Delta}{\partial x} = \Theta_2(x)m_{br0}\frac{\partial^2 w_{\mathrm{h}}}{\partial t^2}, \tag{17}$$

$$\frac{\partial\Theta_1(x)\widetilde{M}_\Delta}{\partial x} - \Theta_1(x)\widetilde{Q}_\Delta = \Theta_2(x)m_{br1}\frac{\partial^2 u_0}{\partial t^2} + \Theta_2(x)m_{br2}\frac{\partial^2\psi_{\mathrm{c}}}{\partial t^2} \tag{18}$$

and the boundary conditions

$$\begin{cases} u_0 = 0 \quad \text{or} \quad \Theta_1(x)\widetilde{N}_x = 0, \\ w_{\mathrm{h}} = 0 \quad \text{or} \quad \widetilde{Q}_\Delta = 0, \\ \psi_{\mathrm{c}} = 0 \quad \text{or} \quad \Theta_1(x)\widetilde{M}_\Delta = 0, \\ \dfrac{\partial w_{\mathrm{h}}}{\partial x} = 0 \quad \text{or} \quad \widetilde{Q}_\Delta = 0. \end{cases} \tag{19}$$

Substituting Eq. (10) into Eqs. (16)–(18) yields the dynamic equations in terms of u_0, w_{h}, and ψ_{c} as follows:

$$\begin{aligned} &B^1_{xx}\Big(\frac{\partial^2 u_0}{\partial x^2}\Theta_1(x) + \frac{\partial u_0}{\partial x}\Theta_1'(x)\Big) + B^2_{xx}\Big(\frac{\partial^2\psi_{\mathrm{c}}}{\partial x^2}\Theta_1(x) + \frac{\partial\psi_{\mathrm{c}}}{\partial x}\Theta_1'(x)\Big) \\ &= \Theta_2(x)\Big(m_{br0}\frac{\partial^2 u_0}{\partial t^2} + m_{br1}\frac{\partial^2\psi_{\mathrm{c}}}{\partial t^2}\Big), \end{aligned} \tag{20}$$

$$D_{55}(x)\widetilde{k}_{\mathrm{s}}\Big(\frac{\partial^2 w_{\mathrm{h}}}{\partial x^2} + \frac{\partial\psi_{\mathrm{c}}}{\partial x}\Big) + D'_{55}(x)\widetilde{k}_{\mathrm{s}}\Big(\frac{\partial w_{\mathrm{h}}}{\partial x} + \psi_{\mathrm{c}}\Big) = \Theta_2(x)m_{br0}\frac{\partial^2 w_{\mathrm{h}}}{\partial t^2}, \tag{21}$$

$$\begin{aligned} &B^2_{xx}\Big(\frac{\partial^2 u_0}{\partial x^2}\Theta_1(x) + \frac{\partial u_0}{\partial x}\Theta_1'(x)\Big) + B^3_{xx}\Big(\frac{\partial^2\psi_{\mathrm{c}}}{\partial x^2}\Theta_1(x) + \frac{\partial\psi_{\mathrm{c}}}{\partial x}\Theta_1'(x)\Big) - D_{55}(x)\widetilde{k}_{\mathrm{s}}\Big(\frac{\partial w_{\mathrm{h}}}{\partial x} + \psi_{\mathrm{c}}\Big) \\ &= \Theta_2(x)\Big(m_{br1}\frac{\partial^2 u_0}{\partial t^2} + m_{br2}\frac{\partial^2\psi_{\mathrm{c}}}{\partial t^2}\Big). \end{aligned} \tag{22}$$

Assume that the material properties change exponentially in the axial orientation. Then, we obtain

$$\Theta_1(x) = \Theta_2(x) = \Theta_3(x) = \mathrm{e}^{\frac{\beta}{L}x}, \tag{23}$$

where β stands for the axial FGM index. Substituting Eq. (23) into Eqs. (20)–(22) yields

$$\begin{aligned} &B^1_{xx}\Big(\frac{\partial^2 u_0}{\partial x^2}\mathrm{e}^{\frac{\beta}{L}x} + \frac{\partial u_0}{\partial x}\mathrm{e}^{\frac{\beta}{L}x}\frac{\beta}{L}\Big) + B^2_{xx}\Big(\frac{\partial^2\psi_{\mathrm{c}}}{\partial x^2}\mathrm{e}^{\frac{\beta}{L}x} + \frac{\partial\psi_{\mathrm{c}}}{\partial x}\mathrm{e}^{\frac{\beta}{L}x}\frac{\beta}{L}\Big) \\ &= \mathrm{e}^{\frac{\beta}{L}x}\Big(m_{br0}\frac{\partial^2 u_0}{\partial t^2} + m_{br1}\frac{\partial^2\psi_{\mathrm{c}}}{\partial t^2}\Big), \end{aligned} \tag{24}$$

$$D_{55}(x)\widetilde{k}_{\mathrm{s}}\Big(\frac{\partial^2 w_{\mathrm{h}}}{\partial x^2} + \frac{\partial\psi_{\mathrm{c}}}{\partial x}\Big) + D'_{55}(x)\widetilde{k}_{\mathrm{s}}\Big(\frac{\partial w_{\mathrm{h}}}{\partial x} + \psi_{\mathrm{c}}\Big) = \mathrm{e}^{\frac{\beta}{L}x}m_{br0}\frac{\partial^2 w_{\mathrm{h}}}{\partial t^2}, \tag{25}$$

$$\begin{aligned} &B^2_{xx}\Big(\frac{\partial^2 u_0}{\partial x^2}\mathrm{e}^{\frac{\beta}{L}x} + \frac{\partial u_0}{\partial x}\mathrm{e}^{\frac{\beta}{L}x}\frac{\beta}{L}\Big) + B^3_{xx}\Big(\frac{\partial^2\psi_{\mathrm{c}}}{\partial x^2}\mathrm{e}^{\frac{\beta}{L}x} + \frac{\partial\psi_{\mathrm{c}}}{\partial x}\mathrm{e}^{\frac{\beta}{L}x}\frac{\beta}{L}\Big) - D_{55}(x)\widetilde{k}_{\mathrm{s}}\Big(\frac{\partial w_{\mathrm{h}}}{\partial x} + \psi_{\mathrm{c}}\Big) \\ &= \mathrm{e}^{\frac{\beta}{L}x}\Big(m_{br1}\frac{\partial^2 u_0}{\partial t^2} + m_{br2}\frac{\partial^2\psi_{\mathrm{c}}}{\partial t^2}\Big). \end{aligned} \tag{26}$$

Let us introduce the following dimensionless variables:

$$\begin{cases} \overline{u}_{\mathrm{g}} = \dfrac{u_0}{L\pi}, \quad \overline{w}_{\mathrm{hg}} = \dfrac{w_{\mathrm{h}}}{L}, \quad \overline{\xi} = \pi\dfrac{x}{L}, \quad \overline{\phi}_{\mathrm{cg}} = \dfrac{\psi_{\mathrm{c}}}{\pi}, \quad \overline{\beta} = \dfrac{\beta}{\pi}, \\ (\chi_1, \chi_2, \chi_3) = (B^1_{xx}, B^2_{xx}, B^3_{xx})\dfrac{1}{B^0_{xx}}, \quad G_{mm} = \dfrac{D_{55}L^2}{D^0_{xx}}, \quad \lambda_{10} = \dfrac{m_{br0}}{m^0_{br0}\pi^2}, \\ (\lambda_{11}, \lambda_{12}) = \Big(\dfrac{m_{br1}}{L}, \dfrac{m_{br2}}{L^2}\Big)\dfrac{1}{m^0_{br0}}, \quad \tau = \dfrac{\pi t}{L^2}\sqrt{\dfrac{B^0_{xx}}{m^0_{br0}}}, \end{cases} \tag{27}$$

where $m^0_{br0} = \int_{\widehat{A}} \rho^{\mathrm{m}} \mathrm{d}\widehat{A}$, and $B^0_{xx} = \int_{\widehat{A}} E^{\mathrm{m}} z^2 \mathrm{d}\widehat{A}$. Substituting Eq. (27) into Eqs. (24)–(26) yields the dimensionless governing equations for the 3D FGM Timoshenko tube as follows:

$$\chi_1 \mathrm{e}^{\overline{\beta}\,\overline{\xi}}\Big(\frac{\partial^2 \overline{u}_{\mathrm{g}}}{\partial \overline{\xi}^2} + \frac{\partial \overline{u}_{\mathrm{g}}}{\partial \overline{\xi}}\overline{\beta}\Big) + \chi_2 \mathrm{e}^{\overline{\beta}\,\overline{\xi}}\Big(\frac{\partial^2 \overline{\phi}_{\mathrm{cg}}}{\partial \overline{\xi}^2} + \frac{\partial \overline{\phi}_{\mathrm{cg}}}{\partial \overline{\xi}}\overline{\beta}\Big) = \mathrm{e}^{\overline{\beta}\,\overline{\xi}}\Big(\lambda_{10}\frac{\partial^2 \overline{u}_{\mathrm{g}}}{\partial \tau^2} + \lambda_{11}\frac{\partial^2 \overline{\phi}_{\mathrm{cg}}}{\partial \tau^2}\Big), \tag{28}$$

$$G_{mm}\widetilde{k}_{\mathrm{s}}\Big(\frac{\partial^2 \overline{w}_{\mathrm{hg}}}{\partial \overline{\xi}^2} + \frac{\partial \overline{\phi}_{\mathrm{cg}}}{\partial \overline{\xi}}\Big) + \frac{\partial G_{mm}}{\partial \overline{\xi}}\widetilde{k}_{\mathrm{s}}\overline{\beta}\Big(\frac{\partial \overline{w}_{\mathrm{hg}}}{\partial \overline{\xi}} + \overline{\phi}_{\mathrm{cg}}\Big) = \mathrm{e}^{\overline{\beta}\,\overline{\xi}}\lambda_{10}\frac{\partial^2 \overline{w}_{\mathrm{hg}}}{\partial \tau^2}, \tag{29}$$

$$\begin{aligned} &\chi_2 \mathrm{e}^{\overline{\beta}\,\overline{\xi}}\Big(\frac{\partial^2 \overline{u}_{\mathrm{g}}}{\partial \overline{\xi}^2} + \frac{\partial \overline{u}_{\mathrm{g}}}{\partial \overline{\xi}}\overline{\beta}\Big) + \chi_3 \mathrm{e}^{\overline{\beta}\,\overline{\xi}}\Big(\frac{\partial^2 \overline{\phi}_{\mathrm{cg}}}{\partial \overline{\xi}^2} + \frac{\partial \overline{\phi}_{\mathrm{cg}}}{\partial \overline{\xi}}\overline{\beta}\Big) - \widetilde{k}_{\mathrm{s}}G_{mm}\Big(\frac{\partial \overline{w}_{\mathrm{hg}}}{\partial \overline{\xi}} + \overline{\phi}_{\mathrm{cg}}\Big) \\ &= \mathrm{e}^{\overline{\beta}\,\overline{\xi}}\Big(\lambda_{11}\frac{\partial^2 \overline{u}_{\mathrm{g}}}{\partial \tau^2} + \lambda_{12}\frac{\partial^2 \overline{\phi}_{\mathrm{cg}}}{\partial \tau^2}\Big). \end{aligned} \tag{30}$$

From Eq. (27), one can divide the end supports of Eq. (19) into the following cases:

$$\begin{cases} \overline{u}_{\mathrm{g}}(0,\tau) = \overline{u}_{\mathrm{g}}(1,\tau) = 0, \quad \overline{w}_{\mathrm{hg}}(0,\tau) = \overline{w}_{\mathrm{hg}}(1,\tau) = 0, \\ \dfrac{\partial \overline{w}_{\mathrm{hg}}(0,\tau)}{\partial \overline{\xi}} = \dfrac{\partial \overline{w}_{\mathrm{hg}}(1,\tau)}{\partial \overline{\xi}} = 0, \quad \overline{\phi}_{\mathrm{cg}}(0,\tau) = \overline{\phi}_{\mathrm{cg}}(1,\tau) = 0 \end{cases} \tag{31}$$

for a clamped-clamped (C-C) Timoshenko tube,

$$\begin{cases} \overline{u}_{\mathrm{g}}(0,\tau) = \overline{u}_{\mathrm{g}}(1,\tau) = 0, \quad \overline{w}_{\mathrm{hg}}(0,\tau) = \overline{w}_{\mathrm{hg}}(1,\tau) = 0, \\ \dfrac{\partial^2 \overline{w}_{\mathrm{hg}}(0,\tau)}{\partial \overline{\xi}^2} = \dfrac{\partial^2 \overline{w}_{\mathrm{hg}}(1,\tau)}{\partial \overline{\xi}^2} = 0, \quad \dfrac{\partial \overline{\phi}_{\mathrm{cg}}(0,\tau)}{\partial \overline{\xi}} = \dfrac{\partial \overline{\phi}_{\mathrm{cg}}(1,\tau)}{\partial \overline{\xi}} = 0 \end{cases} \tag{32}$$

for a hinged-hinged (H-H) Timoshenko tube,

$$\begin{cases} \overline{u}_{\mathrm{g}}(0,\tau) = \overline{u}_{\mathrm{g}}(1,\tau) = 0, \quad \overline{w}_{\mathrm{hg}}(0,\tau) = \overline{w}_{\mathrm{hg}}(1,\tau) = 0, \\ \dfrac{\partial \overline{w}_{\mathrm{hg}}(0,\tau)}{\partial \overline{\xi}} = \dfrac{\partial^2 \overline{w}_{\mathrm{hg}}(1,\tau)}{\partial \overline{\xi}^2} = 0, \quad \overline{\phi}_{\mathrm{cg}}(0,\tau) = \dfrac{\partial \overline{\phi}_{\mathrm{cg}}(1,\tau)}{\partial \overline{\xi}} = 0 \end{cases} \tag{33}$$

for a clamped-hinged (C-H) Timoshenko tube, and

$$\begin{cases} \overline{u}_{\mathrm{g}}(0,\tau) = \dfrac{\partial^2 \overline{u}_{\mathrm{g}}(1,\tau)}{\partial \overline{\xi}^2} = 0, \quad \overline{w}_{\mathrm{hg}}(0,\tau) = \dfrac{\partial^2 \overline{w}_{\mathrm{hg}}(1,\tau)}{\partial \overline{\xi}^2} = 0, \\ \dfrac{\partial \overline{w}_{\mathrm{hg}}(0,\tau)}{\partial \overline{\xi}} = \dfrac{\partial^3 \overline{w}_{\mathrm{hg}}(1,\tau)}{\partial \overline{\xi}^3} = 0, \quad \overline{\phi}_{\mathrm{cg}}(0,\tau) = \dfrac{\partial^2 \overline{\phi}_{\mathrm{cg}}(1,\tau)}{\partial \overline{\xi}^2} = 0 \end{cases} \tag{34}$$

for a clamped-free (C-F) Timoshenko tube.

3 Solution procedure

3.1 DQM

The DQM is put forward for conducting the solving procedure. According to the DQM, $\overline{u}_{\mathrm{g}}$, $\overline{w}_{\mathrm{hg}}$, $\overline{\phi}_{\mathrm{cg}}$, and their mth derivatives can be expressed as follows:

$$(\overline{u}_{\mathrm{g}}, \overline{w}_{\mathrm{hg}}, \overline{\phi}_{\mathrm{cg}}) = \sum_{j=1}^{N} \kappa_j(\overline{\xi})(\overline{u}_{\mathrm{g}}^j, \overline{w}_{\mathrm{hg}}^j, \overline{\phi}_{\mathrm{cg}}^j), \tag{35}$$

$$\frac{\partial^m}{\partial \overline{\xi}^m}(\overline{u}_{\mathrm{g}}, \overline{w}_{\mathrm{hg}}, \overline{\phi}_{\mathrm{cg}})_{\overline{\xi}=\overline{\xi}_k} = \sum_{j=1}^{N} \Xi_{kj}^{(m)}(\overline{u}_{\mathrm{g}}^j, \overline{w}_{\mathrm{hg}}^j, \overline{\phi}_{\mathrm{cg}}^j), \tag{36}$$

where N is the number of mesh points, $\kappa_j(\overline{\xi})$ means Lagrange interpolation polynomials, and $\Xi_{kj}^{(m)}$ is the mth-order weighting coefficient in which the mathematical formula can be presented by the previous literature[25]. By virtue of the Chebyshev-Gauss-Lobatto technique, we obtain the distribution of mesh points as follows:

$$\overline{\xi}_k = \frac{1}{2}\Big(1 - \cos\frac{k\pi}{N-1}\Big), \quad k = 1, 2, \cdots, N. \tag{37}$$

Substituting Eqs. (35) and (36) into Eqs. (28)–(30) yields a series of ordinary differential equations as follows:

$$\begin{aligned}
&\chi_1 \mathrm{e}^{\overline{\beta}\,\overline{\xi}_k}\Big(\sum_{j=1}^{N}\Xi_{kj}^{(2)}\overline{u}_{\mathrm{g}}^j + \overline{\beta}\sum_{j=1}^{N}\Xi_{kj}^{(1)}\overline{u}_{\mathrm{g}}^j\Big) + \chi_2 \mathrm{e}^{\overline{\beta}\,\overline{\xi}_k}\Big(\sum_{j=1}^{N}\Xi_{kj}^{(2)}\overline{\phi}_{\mathrm{cg}}^j + \overline{\beta}\sum_{j=1}^{N}\Xi_{kj}^{(1)}\overline{\phi}_{\mathrm{cg}}^j\Big) \\
&= \mathrm{e}^{\overline{\beta}\,\overline{\xi}_k}(\lambda_{10}\ddot{\overline{u}}_{\mathrm{g}}^k + \lambda_{11}\ddot{\overline{\phi}}_{\mathrm{cg}}^k),
\end{aligned} \tag{38}$$

$$\begin{aligned}
&G_{mm}\widetilde{k}_{\mathrm{s}}\Big(\sum_{j=1}^{N}\Xi_{kj}^{(2)}\overline{w}_{\mathrm{hg}}^j + \sum_{j=1}^{N}\Xi_{kj}^{(1)}\overline{\phi}_{\mathrm{cg}}^j\Big) + \sum_{j=1}^{N}\Xi_{kj}^{(1)}G_{mm}^j\widetilde{k}_{\mathrm{s}}\overline{\beta}\Big(\sum_{j=1}^{N}\Xi_{kj}^{(1)}\overline{w}_{\mathrm{hg}}^j + \overline{\phi}_{\mathrm{cg}}^k\Big) \\
&= \mathrm{e}^{\overline{\beta}\,\overline{\xi}_k}\lambda_{10}\ddot{\overline{w}}_{\mathrm{hg}}^k,
\end{aligned} \tag{39}$$

$$\begin{aligned}
&\chi_2 \mathrm{e}^{\overline{\beta}\,\overline{\xi}_k}\Big(\sum_{j=1}^{N}\Xi_{kj}^{(2)}\overline{u}_{\mathrm{g}}^j + \overline{\beta}\sum_{j=1}^{N}\Xi_{kj}^{(1)}\overline{u}_{\mathrm{g}}^j\Big) + \chi_3 \mathrm{e}^{\overline{\beta}\,\overline{\xi}_k}\Big(\sum_{j=1}^{N}\Xi_{kj}^{(2)}\overline{\phi}_{\mathrm{cg}}^j + \overline{\beta}\sum_{j=1}^{N}\Xi_{kj}^{(1)}\overline{\phi}_{\mathrm{cg}}^j\Big) \\
&- \widetilde{k}_{\mathrm{s}}G_{mm}\Big(\sum_{j=1}^{N}\Xi_{kj}^{(1)}\overline{w}_{\mathrm{hg}}^j + \overline{\phi}_{\mathrm{cg}}^k\Big) = \mathrm{e}^{\overline{\beta}\,\overline{\xi}_k}(\lambda_{11}\ddot{\overline{u}}_{\mathrm{g}}^k + \lambda_{12}\ddot{\overline{\phi}}_{\mathrm{cg}}^k),
\end{aligned} \tag{40}$$

where the over dot stands for the differentiation with respect to τ. With the similar procedure, the boundary conditions can be discretized. Define the unknown vector as follows:

$$\overline{\Lambda} = ((\overline{u}_{\mathrm{g}}^j)^{\mathrm{T}}, (\overline{w}_{\mathrm{hg}}^j)^{\mathrm{T}}(\overline{\phi}_{\mathrm{cg}}^j)^{\mathrm{T}})^{\mathrm{T}}, \quad j = 1, 2, \cdots, N. \tag{41}$$

Assembling the matrices corresponding to the end supports and Eqs. (38)–(40) yields

$$\overline{M}\,\ddot{\overline{\Lambda}} + \overline{K}\,\overline{\Lambda} = 0, \tag{42}$$

where $\overline{K}$ and $\overline{M}$ are the stiffness and mass matrixes, respectively. Calculating the standard eigenvalue issue, one can obtain the dimensionless natural frequencies and the corresponding mode shapes of the 3D FGM Timoshenko tube.

3.2 Ritz method

To illustrate the correctness of the DQM, we use the Ritz method to determine the natural dynamic characteristics of the 3D FGM Timoshenko tube. Based on Eqs. (7) and (13), the potential energy and the kinetic energy of the tube are transformed into the following forms:

$$\Pi_U = \frac{B_{xx}^0}{2L}\int_0^1 \Theta_1(\xi)\Big(\chi_1\Big(\frac{\partial\overline{u}_{\rm g}}{\partial\overline{\xi}}\Big)^2 + 2\chi_2\frac{\partial\overline{u}_{\rm g}}{\partial\overline{\xi}}\frac{\partial\overline{\phi}_{\rm cg}}{\partial\overline{\xi}} + \chi_3\Big(\frac{\partial\overline{\phi}_{\rm cg}}{\partial\overline{\xi}}\Big)^2\Big) + \Theta_3(\xi)\overline{k}_{\rm s}D_{55}\Big(\Big(\frac{\partial\overline{w}_{\rm hg}}{\partial\overline{\xi}}\Big)^2 + 2\frac{\partial\overline{w}_{\rm hg}}{\partial\overline{\xi}}\overline{\phi}_{\rm cg} + \overline{\phi}_{\rm cg}^2\Big)\mathrm{d}\overline{\xi}, \tag{43}$$

$$\Pi_T = \frac{B_{xx}^0}{2L}\int_0^1 \Theta_2(\xi)\Big(\lambda_{10}\Big(\frac{\partial\overline{u}_{\rm g}}{\partial\tau}\Big)^2 + 2\lambda_{11}\frac{\partial\overline{u}_{\rm g}}{\partial\tau}\frac{\partial\overline{\phi}_{\rm cg}}{\partial\tau} + \lambda_{12}\Big(\frac{\partial\overline{\phi}_{\rm cg}}{\partial\tau}\Big)^2 + \lambda_{10}\Big(\frac{\partial\overline{w}_{\rm hg}}{\partial\tau}\Big)^2\Big)\mathrm{d}\overline{\xi}. \tag{44}$$

The energy function of the 3D FGM tube can be written as

$$\Gamma = \Pi_U - \Pi_T. \tag{45}$$

To apply the standard Ritz procedure, the axial, transverse, and rotational deflections of the tube are approximated by a series of auxiliary functions as follows:

$$\overline{w}_{\rm hg} = \sum_{m=1}^{N} A_m(\tau)\mu_{mw}(\overline{\xi}), \quad \mu_{mw}(\overline{\xi}) = \eta_w(\overline{\xi})\overline{\xi}^{m-1}, \tag{46}$$

$$\overline{u}_{\rm g} = \sum_{m=1}^{N} B_m(\tau)\mu_{mu}(\overline{\xi}), \quad \mu_{mu}(\overline{\xi}) = \eta_u(\overline{\xi})\overline{\xi}^{m-1}, \tag{47}$$

$$\overline{\phi}_{\rm cg} = \sum_{m=1}^{N} C_m(\tau)\mu_{m\psi}(\overline{\xi}), \quad \mu_{m\psi}(\overline{\xi}) = \eta_\psi(\overline{\xi})\overline{\xi}^{m-1}, \tag{48}$$

where $A_m(\tau)$, $B_m(\tau)$, and $C_m(\tau)$ stand for unknown time-dependent coefficients. η_w, η_u, and η_ψ are the Ritz trial functions adopted to satisfy the geometric end supports. The Ritz trial functions can be written as follows:

$$\eta_w(\overline{\xi}) = \overline{\xi}^{p_w}(1-\overline{\xi})^{q_w}, \quad \eta_u(\overline{\xi}) = \overline{\xi}^{p_u}(1-\overline{\xi})^{q_u}, \quad \eta_\psi(\overline{\xi}) = \overline{\xi}^{p_\psi}(1-\overline{\xi})^{q_\psi}, \tag{49}$$

where p_m and q_m $(m = w, u, \psi)$ denote the exponents corresponding to the boundary conditions. Table 1 gives the boundary exponents for different supported edges.

Table 1 Various values of the boundary exponents for different supported edges

Boundary condition	Left end			Right end		
	p_w	p_u	p_ψ	q_w	q_u	q_ψ
H-H tube	1	1	0	1	0	0
C-C tube	1	1	1	1	1	1
C-H tube	1	1	1	1	0	0
C-F tube	1	1	1	0	0	0

Application of the Lagrange equations to the 3D FGM Timoshenko tube yields

$$\frac{\mathrm{d}}{\mathrm{d}t}\Big(\frac{\partial\Gamma}{\partial\dot{\vartheta}_m}\Big) - \frac{\partial\Gamma}{\partial\vartheta_m} = 0, \quad m = 1, 2, \cdots, 3N, \tag{50}$$

where

$$\vartheta_m = \begin{cases} A_m, & m = 1, 2, \cdots, N, \\ B_{m-N}, & m = N+1, N+2, \cdots, 2N, \\ C_{m-2N}, & m = 2N+1, 2N+2, \cdots, 3N. \end{cases} \tag{51}$$

Substituting Eqs. (43)–(45) into Eq. (50) yields

$$\begin{pmatrix} K_1 & 0 & K_3 \\ 0 & K_5 & K_6 \\ K_7 & K_8 & K_9 \end{pmatrix} \begin{pmatrix} A(\tau) \\ B(\tau) \\ C(\tau) \end{pmatrix} + \begin{pmatrix} M_1 & 0 & 0 \\ 0 & M_5 & M_6 \\ 0 & M_8 & M_9 \end{pmatrix} \begin{pmatrix} \ddot{A}(\tau) \\ \ddot{B}(\tau) \\ \ddot{C}(\tau) \end{pmatrix} = 0, \tag{52}$$

where K_m and M_m are the stiffness and mass matrices, respectively. It is mentioned here that the stiffness and mass matrices are symmetric and in the size of $N \times N$. Their elements are listed as follows:

$$\begin{cases} K_1^{lm} = \displaystyle\int_0^1 \Theta_3(\bar{\xi}) \widetilde{k}_{\mathrm{s}} D_{55} \frac{\partial \mu_{lw}}{\partial \bar{\xi}} \frac{\partial \mu_{mw}}{\partial \bar{\xi}} \mathrm{d}\bar{\xi}, \quad K_3^{lm} = \int_0^1 \Theta_3(\bar{\xi}) \widetilde{k}_{\mathrm{s}} D_{55} \frac{\partial \mu_{lw}}{\partial \bar{\xi}} \mu_{m\psi} \mathrm{d}\bar{\xi}, \\ K_5^{lm} = \displaystyle\int_0^1 \Theta_1(\bar{\xi}) \chi_1 \frac{\partial \mu_{lu}}{\partial \bar{\xi}} \frac{\partial \mu_{mu}}{\partial \bar{\xi}} \mathrm{d}\bar{\xi}, \quad K_6^{lm} = \int_0^1 \Theta_1(\bar{\xi}) \chi_2 \frac{\partial \mu_{lu}}{\partial \bar{\xi}} \frac{\partial \mu_{m\psi}}{\partial \bar{\xi}} \mathrm{d}\bar{\xi}, \\ K_7^{lm} = \displaystyle\int_0^1 \Theta_3(\bar{\xi}) \widetilde{k}_{\mathrm{s}} D_{55} \mu_{l\psi} \frac{\partial \mu_{mw}}{\partial \bar{\xi}} \mathrm{d}\bar{\xi}, \quad K_8^{lm} = \int_0^1 \Theta_1(\bar{\xi}) \chi_2 \frac{\partial \mu_{l\psi}}{\partial \bar{\xi}} \frac{\partial \mu_{mu}}{\partial \bar{\xi}} \mathrm{d}\bar{\xi}, \\ K_9^{lm} = \displaystyle\int_0^1 \Theta_1(\bar{\xi}) \chi_3 \frac{\partial \mu_{l\psi}}{\partial \bar{\xi}} \frac{\partial \mu_{m\psi}}{\partial \bar{\xi}} \mathrm{d}\bar{\xi} + \int_0^1 \Theta_3(\bar{\xi}) \widetilde{k}_{\mathrm{s}} D_{55} \mu_{l\psi} \mu_{m\psi} \mathrm{d}\bar{\xi}, \end{cases} \tag{53}$$

$$\begin{cases} M_1^{lm} = \displaystyle\int_0^1 \Theta_2(\bar{\xi}) \lambda_{10} \mu_{lw} \mu_{mw} \mathrm{d}\bar{\xi}, \quad M_5^{lm} = \int_0^1 \Theta_2(\bar{\xi}) \lambda_{10} \mu_{lu} \mu_{mu} \mathrm{d}\bar{\xi}, \\ M_6^{lm} = \displaystyle\int_0^1 \Theta_2(\bar{\xi}) \lambda_{11} \mu_{lu} \mu_{m\psi} \mathrm{d}\bar{\xi}, \quad M_8^{lm} = \int_0^1 \Theta_2(\bar{\xi}) \lambda_{11} \mu_{l\psi} \mu_{mu} \mathrm{d}\bar{\xi}, \\ M_9^{lm} = \displaystyle\int_0^1 \Theta_2(\bar{\xi}) \lambda_{12} \mu_{l\psi} \mu_{m\psi} \mathrm{d}\bar{\xi}. \end{cases} \tag{54}$$

Based on Eq. (52), the QR decomposition method in the MATLAB software is used to solve the standard eigenvalue problems. Then, we can determine the natural frequencies of the 3D FGM Timoshenko tube under different boundary conditions.

3.3 FEM

We also use the FEM based on the COMSOL software to solve the free vibration of the 3D FGM Timoshenko tube. The detailed steps are as follows.

(i) According to the geometric parameters used in the DQM, we establish a 3D entity model for the circular cylinders by virtue of Boolean operations. Then, the material properties are set with the help of importing the mixture rule that the volume fraction of body varies along the axial, radial, and circumferential directions in the built-in functions.

(ii) The constraint conditions are imposed in the end supports of the Timoshenko tube, which should be satisfied by different boundary conditions, e.g., H-H, C-H, C-C, and C-F. In order to improve the calculated efficiency and accuracy, we take the advantage of the triangular mesh uniformly distributed in the radial direction to carry out the grid division.

(iii) On the basis of Eqs. (1) and (2), we use the eigenfrequency and modalities in the COMSOL software to calculate the first- and second-order frequencies and the corresponding mode shapes of the 3D FGM tube.

4 Numerical results

In this section, numerical discussions are carried out to study the natural dynamic characteristics of the 3D FGM Timoshenko tube with the general supported edges. In the simulation procedure, $R_{\mathrm{i}} = 0.002\,5\,\mathrm{m}$, and $R_{\mathrm{o}} = 0.005\,\mathrm{m}$. The 3D FGM Timoshenko tube are made of graded composites of steel (SUS304) and silicon nitride (Si_3N_4) with the following material properties: $E^{\mathrm{m}} = 207.7$ GPa, $E^{\mathrm{c}} = 322.2$ GPa, $\rho^{\mathrm{m}} = 8\,160\,\mathrm{kg}\cdot\mathrm{m}^{-3}$, $\rho^{\mathrm{c}} = 2\,370\,\mathrm{kg}\cdot\mathrm{m}^{-3}$, $\nu^{\mathrm{m}} = 0.31$, and $\nu^{\mathrm{c}} = 0.24$. It is also pointed out that the shear correction factor $\widetilde{k}_{\mathrm{s}}$ of the Timoshenko tube is chosen as follows[12]:

$$\widetilde{k}_{\mathrm{s}} = \frac{6\Big(\Big(\dfrac{R_{\mathrm{i}}}{R_{\mathrm{o}}}\Big)^2+1\Big)^2(1+\widetilde{\nu})^2}{(7+12\widetilde{\nu}+4\widetilde{\nu}^2)\Big(\Big(\dfrac{R_{\mathrm{i}}}{R_{\mathrm{o}}}\Big)^4+1\Big)+(34+48\widetilde{\nu}+16\widetilde{\nu}^2)\Big(\dfrac{R_{\mathrm{i}}}{R_{\mathrm{o}}}\Big)^2}. \tag{55}$$

4.1 Verification

In order to verify the effectiveness of the natural frequencies and mode shapes calculated by the DQM, we first compare the dimensionless fundamental frequencies of the Timoshenko tube with C-C, H-H, C-H, and C-F end supports obtained by the DQM, FEM, and Ritz method. The results are shown in Table 2. It is shown that the solutions obtained by the three methods are similar, which validates the correctness of the present natural frequency. Figure 2 compares the mode shapes and nephograms of the 3D FGM Timoshenko tube under the H-H boundary condition determined by the DQM with those predicted by the FEM. It is found that the difference between the first two modes in the transverse and rotation directions is considerably small, indicating the effectiveness of the present investigation.

4.2 Parametric study

Tables 3–6 exploit the effects of the axial, radial, and circumferential FGM indexes as well as the length-radius ratio on the dimensionless fundamental frequency of the 3D FGM Timoshenko tube with different end supports. For the C-C 3D FGM Timoshenko tube, one may observe that the dimensionless fundamental frequency increases as the axial FGM index β increases,

Table 2 Comparison of dimensionless fundamental frequencies of the Timoshenko tube with C-C, H-H, C-H, and C-F end supports determined by the DQM, FEM, and Ritz method for different values of the axial, radial, and circumferential FGM indexes ($L/R_{\mathrm{o}} = 20$)

End support	Method	Axial, radial, and circumferential FGM indexes (β, n, k)							
		(0, 0, 0)	(1, 0, 0)	(0, 1, 0)	(0, 0, 1)	(1, 1, 0)	(0, 1, 1)	(1, 0, 1)	(1, 1, 1)
C-C	DQM	48.786 4	49.066 7	31.569 9	29.673 6	31.751 4	25.557 5	29.843 9	25.704 5
	FEM	48.201 5	48.468 5	31.148 3	29.566 8	31.322 3	25.431 8	29.732 7	25.573 2
	Ritz	48.790 4	49.070 8	31.572 6	29.547 1	31.753 9	25.511 5	29.716 8	25.658 0
H-H	DQM	22.478 1	22.245 6	14.569 5	13.671 6	14.418 7	11.786 0	13.530 8	11.664 7
	FEM	22.405 8	22.170 8	14.518 6	13.819 2	14.365 9	11.870 8	13.674 7	11.745 8
	Ritz	22.477 8	22.245 8	14.569 2	13.606 6	14.418 8	11.761 8	13.464 3	11.639 8
C-H	DQM	34.428 1	32.073 1	22.299 0	20.940 0	20.773 5	18.044 7	19.508 0	16.810 0
	FEM	34.183 7	31.841 3	22.123 7	21.034 8	20.607 6	18.076 7	19.596 6	16.838 9
	Ritz	34.428 2	32.072 4	22.299 0	20.845 1	20.772 9	18.009 3	19.418 4	16.776 8
C-F	DQM	8.172 5	6.055 1	5.296 7	4.970 6	3.925 1	4.285 1	3.683 2	3.175 5
	FEM	8.075 1	5.904 3	5.233 3	4.985 1	3.826 5	4.280 7	3.645 5	3.130 3
	Ritz	8.070 9	5.896 3	5.231 3	4.886 2	3.821 9	4.223 6	3.569 7	3.085 7

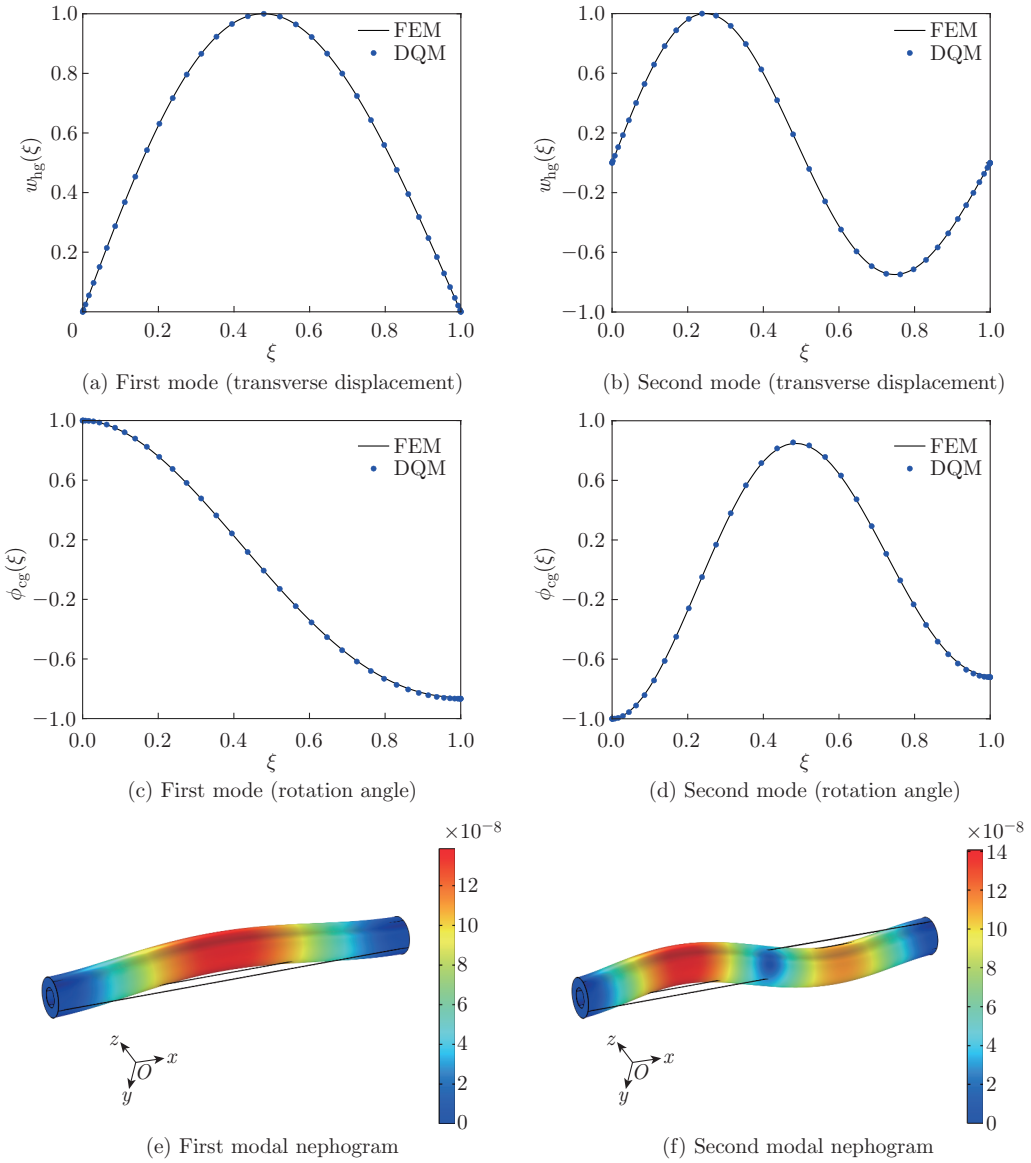

(a) First mode (transverse displacement)

(b) Second mode (transverse displacement)

(c) First mode (rotation angle)

(d) Second mode (rotation angle)

(e) First modal nephogram

(f) Second modal nephogram

Fig. 2 Comparison of the first two mode shapes of the 3D FGM Timoshenko tube with the H-H end support determined by the FEM and DQM ($\beta = 1$, $n = 1$, and $k = 1$) (color online)

but the opposite is achieved for the other supported edges. Another observation is that the increases in both the circumferential FGM index k and the radial FGM index n lead to the lessening of the dimensionless fundamental frequency. From Tables 3–6, it is also seen that the fundamental frequency has an uptrend with respect to the length-to-radius ratio. This means that the rigidity of the Timoshenko tube increases when the length-to-radius ratio increases, indicating that the effective stiffness of the structure improves.

The variations of the first three-order frequencies of the 3D FGM Timoshenko tube as a function of the axial FGM index β under different boundary conditions are explored in Fig. 3. One may recognize that the effects of the index β on higher-order frequencies are the same as those on the fundamental frequency. Moreover, the interesting phenomenon is that, compared with various supported edges, when the stiffness constraint grows from the C-F

Table 3 Dimensionless fundamental frequency of the 3D FGM Timoshenko tube with different values of the length-radius ratio and the axial, radial, and circumferential FGM indexes under the H-H boundary condition

k	n	$(L/R_{\rm o},\beta)$											
		(10, 0)	(10, 0.5)	(10, 1)	(10, 1.5)	(20, 0)	(20, 0.5)	(20, 1)	(20, 1.5)	(30, 0)	(30, 0.5)	(30, 1)	(30, 1.5)
0	0	21.560 1	21.496 0	21.305 0	20.990 2	22.478 1	22.419 7	22.245 6	21.958 5	22.664 1	22.607 5	22.437 3	22.155 1
	1	13.971 9	13.930 5	13.806 7	13.603 1	14.569 5	14.531 8	14.418 7	14.232 7	14.690 7	14.653 6	14.543 1	14.360 2
	5	10.858 6	10.825 9	10.729 8	10.570 8	11.327 3	11.297 8	11.209 8	11.065 3	11.422 2	11.393 3	11.307 8	11.165 8
	20	9.780 4	9.751 5	9.664 8	9.521 5	10.200 1	10.173 7	10.094 6	9.963 9	10.284 9	10.259 2	10.181 9	10.053 7
1	0	13.113 6	13.074 7	12.958 4	12.766 8	13.671 6	13.636 4	13.530 8	13.356 2	13.785 3	13.750 8	13.647 1	13.475 5
	1	11.301 6	11.268 3	11.168 4	11.003 1	11.786 0	11.755 8	11.664 7	11.513 9	11.884 6	11.855 1	11.765 3	11.617 6
	5	10.060 0	10.029 8	9.940 6	9.793 6	10.491 7	10.464 6	10.383 6	10.249 1	10.579 6	10.552 6	10.473 4	10.342 1
	20	9.550 4	9.522 2	9.437 3	9.297 9	9.958 8	9.933 1	9.855 8	9.728 3	10.041 8	10.016 7	9.940 6	9.816 2
2	0	11.579 3	11.544 7	11.442 3	11.273 3	12.071 3	12.039 8	11.946 8	11.792 3	12.171 2	12.141 0	12.049 3	11.897 8
	1	10.565 8	10.534 4	10.440 8	10.286 2	11.017 6	10.989 3	10.903 8	10.763 1	11.109 3	11.081 7	10.998 1	10.859 9
	5	9.799 9	9.771 0	9.683 6	9.540 4	10.219 0	10.192 6	10.113 4	9.982 7	10.304 4	10.278 7	10.200 8	10.072 6
	20	9.471 9	9.444 3	9.360 1	9.221 8	9.875 9	9.850 8	9.774 1	9.647 8	9.958 2	9.933 1	9.858 3	9.734 5

Table 4 Dimensionless fundamental frequency of the 3D FGM Timoshenko tube with different values of the length-radius ratio and the axial, radial, and circumferential FGM indexes under the C-H boundary condition

k	n	$(L/R_{\rm o},\beta)$											
		(10, 0)	(10, 0.5)	(10, 1)	(10, 1.5)	(20, 0)	(20, 0.5)	(20, 1)	(20, 1.5)	(30, 0)	(30, 0.5)	(30, 1)	(30, 1.5)
0	0	31.442 9	30.332 1	29.205 5	28.054 4	34.428 1	33.247 5	32.073 1	30.891 9	35.087 8	33.892 1	32.706 5	31.520 2
	1	20.326 7	19.608 6	18.881 0	18.137 0	22.299 0	21.534 4	20.773 5	20.008 2	22.735 7	21.960 4	21.192 6	20.423 5
	5	15.797 8	15.239 9	14.673 8	14.095 1	17.336 6	16.742 2	16.150 3	15.555 3	17.677 7	17.075 2	16.477 7	15.880 1
	20	14.249 0	13.745 7	13.234 9	12.712 8	15.617 5	15.082 2	14.549 3	14.013 4	15.920 3	15.378 1	14.840 3	14.301 8
1	0	19.124 8	18.449 3	17.763 8	17.063 2	20.940 0	20.222 4	19.508 0	18.789 2	21.341 5	20.614 5	19.893 2	19.171 9
	1	16.459 4	15.878 2	15.288 2	14.685 7	18.044 7	17.426 4	16.810 0	16.191 1	18.395 9	17.768 8	17.147 4	16.525 4
	5	14.653 0	14.135 3	13.610 0	13.073 4	16.063 6	15.512 6	14.964 7	14.413 0	16.375 9	15.817 9	15.264 4	14.710 8
	20	13.921 0	13.429 7	12.930 8	12.420 6	15.250 5	14.727 8	14.207 5	13.684 1	15.544 6	15.014 9	14.489 7	13.964 4
2	0	16.893 0	16.296 1	15.691 0	15.072 1	18.490 8	17.856 8	17.226 0	16.592 0	18.843 9	18.201 8	17.565 3	16.928 2
	1	15.398 2	14.854 1	14.302 4	13.738 2	16.871 6	16.292 9	15.717 4	15.138 1	17.197 1	16.610 9	16.030 3	15.448 5
	5	14.281 7	13.777 1	13.265 1	12.741 7	15.648 3	15.111 7	14.577 6	14.041 0	15.951 1	15.407 0	14.868 5	14.328 8
	20	13.809 8	13.321 6	12.827 1	12.321 3	15.125 5	14.607 1	14.090 7	13.571 7	15.416 4	14.891 1	14.370 3	13.848 8

Table 5 Dimensionless fundamental frequency of the 3D FGM Timoshenko tube with different values of the length-radius ratio and the axial, radial, and circumferential FGM indexes under the C-C boundary condition

k	n	$(L/R_{\rm o},\beta)$											
		(10, 0)	(10, 0.5)	(10, 1)	(10, 1.5)	(20, 0)	(20, 0.5)	(20, 1)	(20, 1.5)	(30, 0)	(30, 0.5)	(30, 1)	(30, 1.5)
0	0	42.364 4	42.416 5	42.576 1	42.848 2	48.786 4	48.856 2	49.066 7	49.422 9	50.351 6	50.426 3	50.652 5	51.033 9
	1	27.314 3	27.348 2	27.451 9	27.627 8	31.569 9	31.615 1	31.751 4	31.981 4	32.611 6	32.660 0	32.806 4	33.053 3
	5	21.232 8	21.259 2	21.339 6	21.475 9	24.544 6	24.579 8	24.686 0	24.865 1	25.356 4	25.394 1	25.507 8	25.700 1
	20	19.178 2	19.202 0	19.274 3	19.397 4	22.122 5	22.153 9	22.249 4	22.410 9	22.841 9	22.875 8	22.978 2	23.151 7
1	0	25.767 3	25.799 4	25.896 1	26.062 0	29.673 6	29.715 7	29.843 9	30.060 6	30.625 5	30.670 7	30.808 3	31.040 8
	1	22.145 1	22.172 7	22.255 7	22.398 3	25.557 5	25.593 9	25.704 5	25.891 1	26.391 9	26.430 8	26.549 6	26.749 4
	5	19.717 3	19.741 8	19.815 9	19.942 8	22.752 0	22.784 7	22.882 7	23.049 2	23.494 1	23.529 3	23.634 2	23.812 6
	20	18.746 5	18.769 8	18.840 1	18.960 8	21.606 6	21.637 4	21.731 0	21.888 7	22.304 7	22.338 0	22.437 9	22.606 9
2	0	22.769 0	22.797 3	22.882 7	23.029 1	26.205 9	26.243 6	26.356 7	26.548 3	27.043 5	27.083 7	27.204 9	27.409 8
	1	20.731 4	20.757 1	20.835 0	20.968 2	23.901 2	23.935 2	24.038 2	24.212 9	24.675 3	24.711 8	24.822 4	25.009 6
	5	19.227 2	19.251 1	19.323 3	19.447 1	22.169 0	22.200 4	22.295 9	22.458 0	22.886 5	22.921 1	23.023 5	23.196 9
	20	18.600 1	18.623 4	18.693 7	18.813 1	21.431 3	21.461 5	21.554 5	21.710 9	22.121 2	22.154 5	22.253 8	22.421 5

end supports to the C-C end supports, the natural frequencies caused by the index β gradually vary from downtrend to uptrend. This means that the constraint of end supports has a significant effect on the frequency variation versus the axial FGM index. The effects of the circumferential and radial FGM indexes on the first three-order frequencies of the 3D FGM Timoshenko tube under various boundary conditions are presented in Figs. 4–5. It is shown that, for all end supports, the downtrend of higher-order frequencies is obtained when the radial and circumferential FGM indexes increase, and the trend becomes more remarkable as the mode order increases.

The effects of the axial, radial, and circumferential FGM indexes on the first two mode shapes (the dimensionless transverse deflection $\overline{w}_{\rm hg}$ and the rotation angle $\overline{\phi}_{\rm cg}$) of the 3D FGM

Table 6 Dimensionless fundamental frequency of the 3D FGM Timoshenko tube with different values of the length-radius ratio and the axial, radial, and circumferential FGM indexes under the C-F boundary condition

k	n	$(L/R_o, \beta)$											
		(10, 0)	(10, 0.5)	(10, 1)	(10, 1.5)	(20, 0)	(20, 0.5)	(20, 1)	(20, 1.5)	(30, 0)	(30, 0.5)	(30, 1)	(30, 1.5)
0	0	8.143 0	7.086 8	6.081 5	5.039 7	8.172 5	7.049 7	6.055 1	5.169 2	8.174 4	7.037 8	6.043 8	5.178 6
	1	5.276 0	4.593 6	3.940 8	3.259 1	5.296 7	4.569 1	3.925 1	3.349 6	5.298 6	4.562 2	3.917 6	3.356 5
	5	4.102 9	3.572 0	3.064 9	2.534 6	4.118 6	3.553 1	3.051 7	2.604 4	4.119 9	3.547 5	3.046 7	2.610 0
	20	3.695 1	3.216 4	2.759 6	2.285 2	3.708 3	3.199 4	2.748 3	2.345 5	3.709 6	3.194 4	2.742 6	2.349 9
1	0	4.953 0	4.310 3	3.698 9	3.065 6	4.970 6	4.287 6	3.683 2	3.144 1	4.971 9	4.280 7	3.676 3	3.149 8
	1	4.269 4	3.716 5	3.188 7	2.639 6	4.285 1	3.697 0	3.175 5	2.710 6	4.287 0	3.690 7	3.169 2	2.715 6
	5	3.800 7	3.308 1	2.838 7	2.349 9	3.814 5	3.291 1	2.826 8	2.412 7	3.815 8	3.285 5	2.821 2	2.417 8
	20	3.607 8	3.139 7	2.694 2	2.231 8	3.621 0	3.123 4	2.682 9	2.290 2	3.621 6	3.118 3	2.677 9	2.294 6
2	0	4.373 1	3.805 7	3.266 0	2.707 4	4.388 8	3.785 6	3.251 5	2.775 9	4.390 1	3.779 3	3.245 9	2.780 9
	1	3.991 1	3.474 0	2.980 7	2.468 7	4.005 5	3.455 8	2.968 2	2.533 4	4.006 8	3.450 1	2.962 5	2.538 4
	5	3.702 1	3.222 0	2.765 2	2.289 6	3.715 2	3.205 1	2.753 3	2.349 9	3.716 5	3.200 0	2.748 3	2.354 3
	20	3.577 6	3.113 9	2.672 2	2.213 6	3.590 8	3.097 6	2.660 9	2.271 4	3.591 5	3.092 6	2.655 9	2.275 8

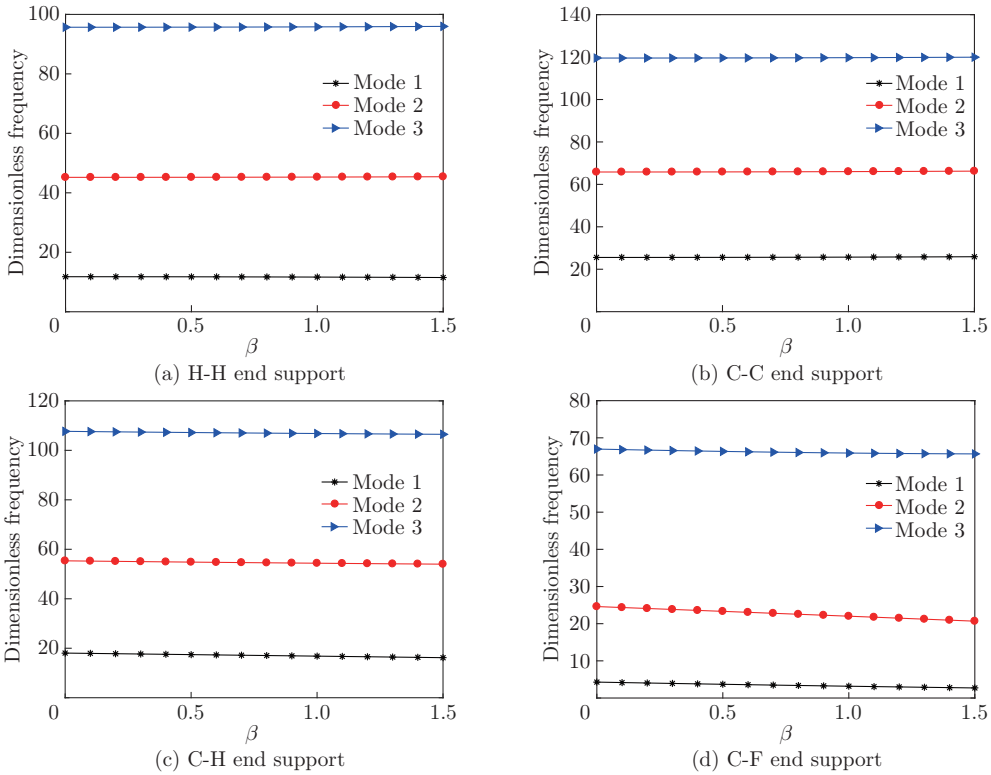

Fig. 3 Variations of the first three-order frequencies of the 3D FGM Timoshenko tube as a function of the axial FGM index with different end supports ($L/R_o = 20$, $n = 1$, and $k = 1$) (color online)

Timoshenko tube with the C-C, H-H, C-H, and C-F end supports are examined in Figs. 6–9. It is observed that, for all types of end supports, the 3D FGM indexes may induce the asymmetric modes of the Timoshenko tube, and the mode shapes for the transverse displacement $\overline{w}_{hg}$ and the rotation angle $\overline{\phi}_{cg}$ significantly depend on the axial FGM index. One could draw a conclusion that the 3D FGM structures conspicuously affect the mode shapes of the Timoshenko tube, which may further tailor/tune the dynamics by 3D FGM composites.

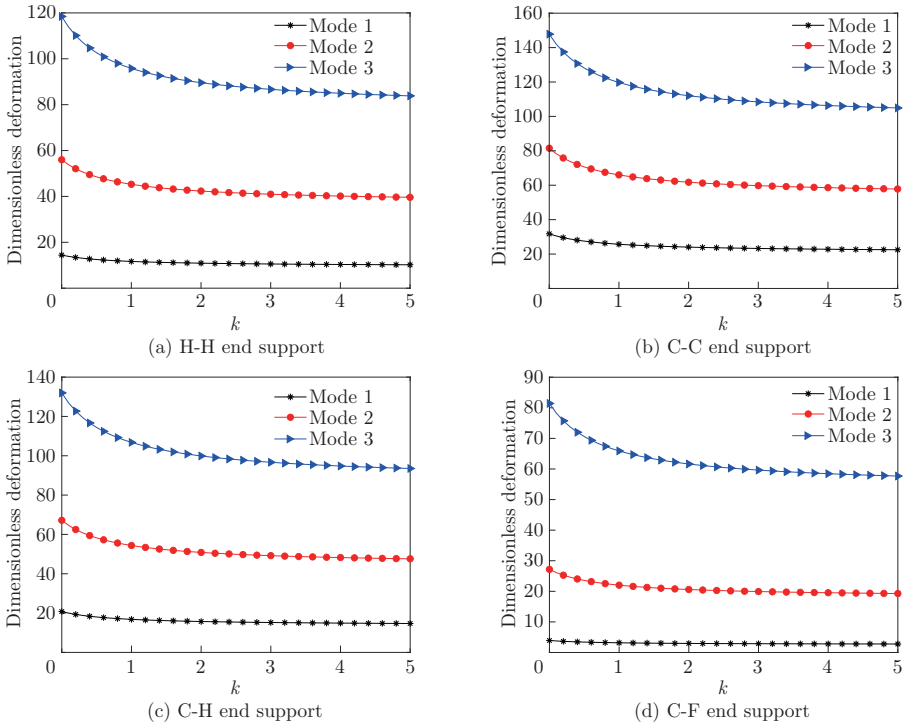

Fig. 4 Variations of the first three-order frequencies of the 3D FGM Timoshenko tube versus the circumferential FGM index with different end supports ($L/R_o = 20$, $\beta = 1$, and $n = 1$) (color online)

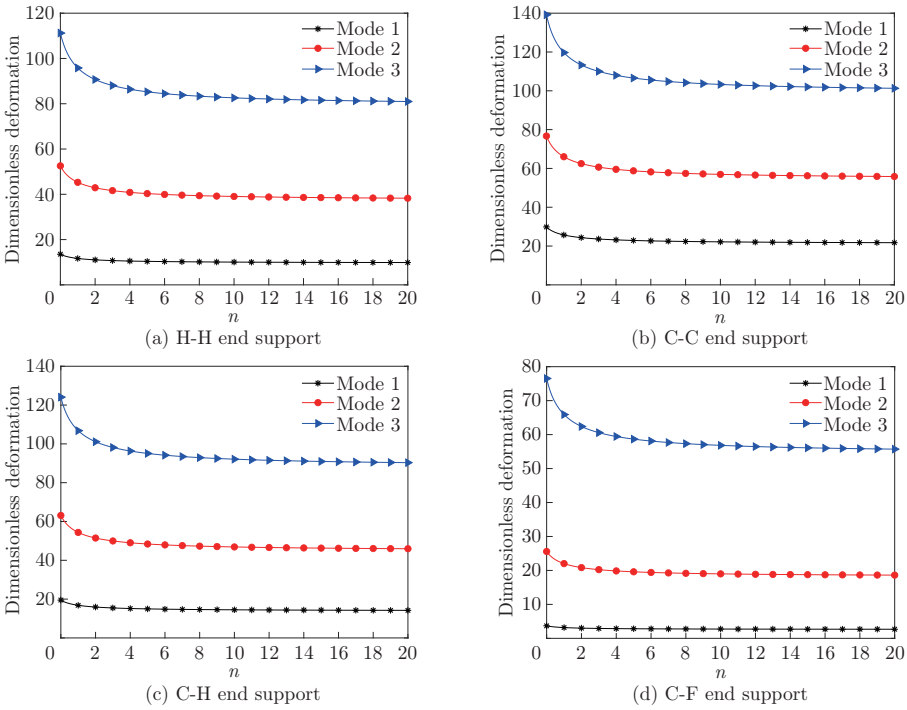

Fig. 5 Variations of the first three-order frequencies of the 3D FGM Timoshenko tube versus the radial FGM index under different boundary conditions ($L/R_o = 20$, $\beta = 1$, and $k = 1$) (color online)

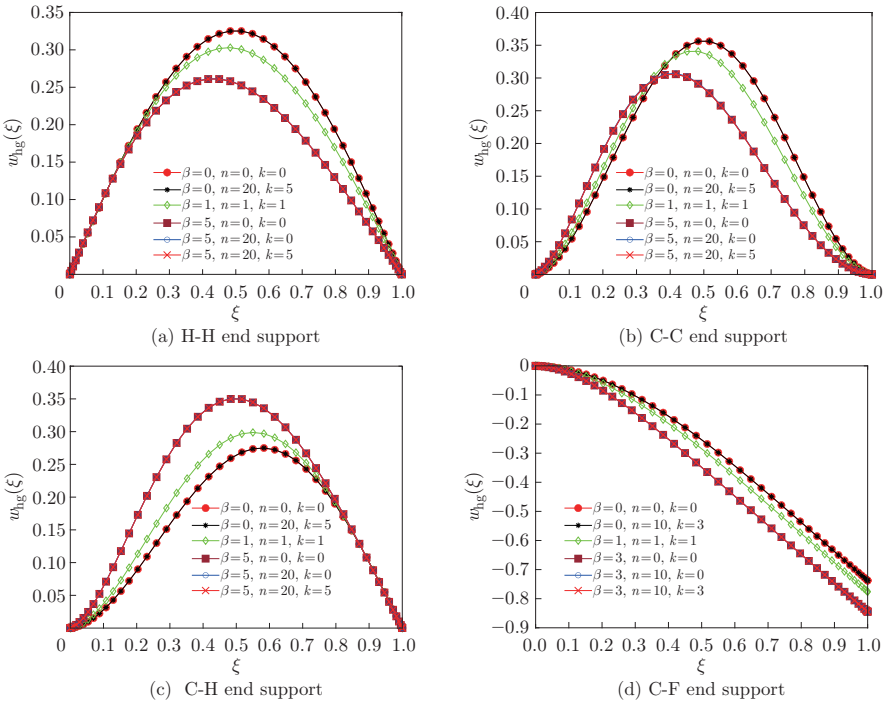

(a) H-H end support (b) C-C end support (c) C-H end support (d) C-F end support

Fig. 6 Effects of the axial, radial, and circumferential FGM indexes on the first mode of the 3D FGM Timoshenko tube (transverse displacement) under different types of boundary conditions ($L/R_o = 20$) (color online)

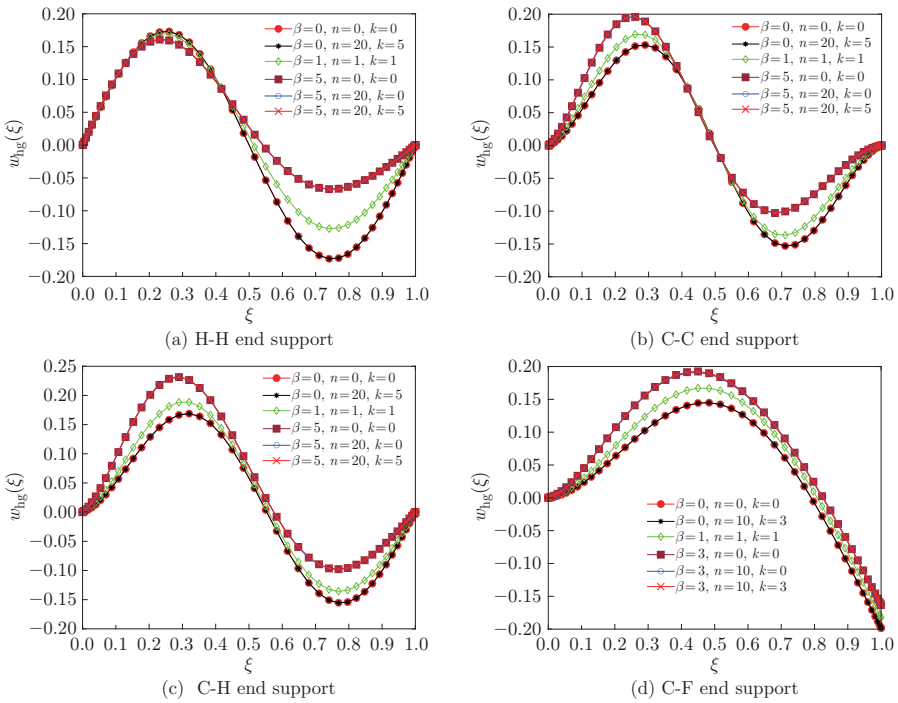

(a) H-H end support (b) C-C end support (c) C-H end support (d) C-F end support

Fig. 7 Effects of the axial, radial, and circumferential FGM indexes on the second mode of the 3D FGM Timoshenko tube (transverse displacement) under different types of boundary conditions ($L/R_o = 20$) (color online)

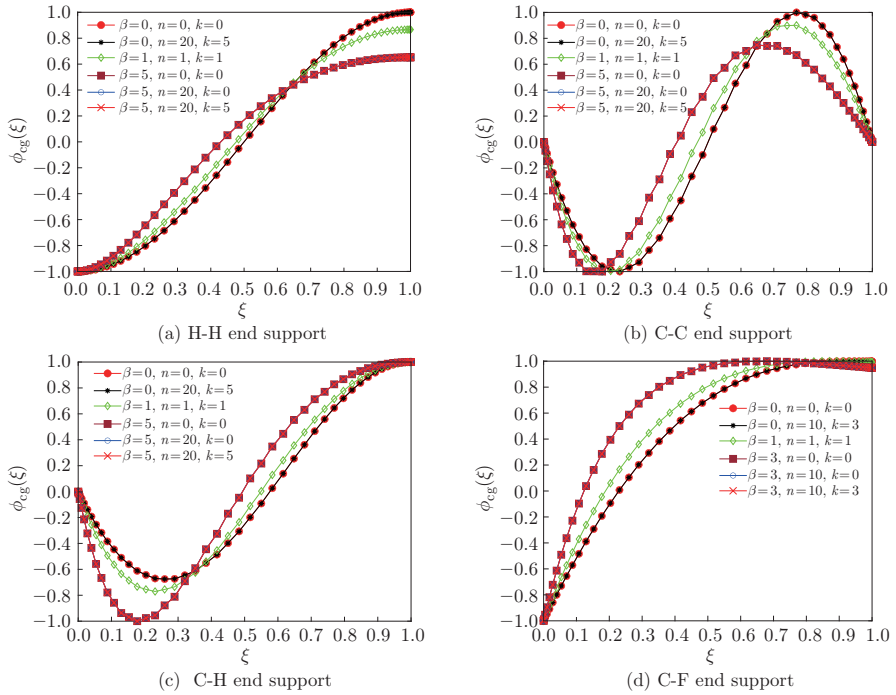

(a) H-H end support (b) C-C end support

(c) C-H end support (d) C-F end support

Fig. 8 Effects of the axial, radial, and circumferential FGM indexes on the first mode of the 3D FGM Timoshenko tube (rotation angle) under different types of boundary conditions ($L/R_o = 20$) (color online)

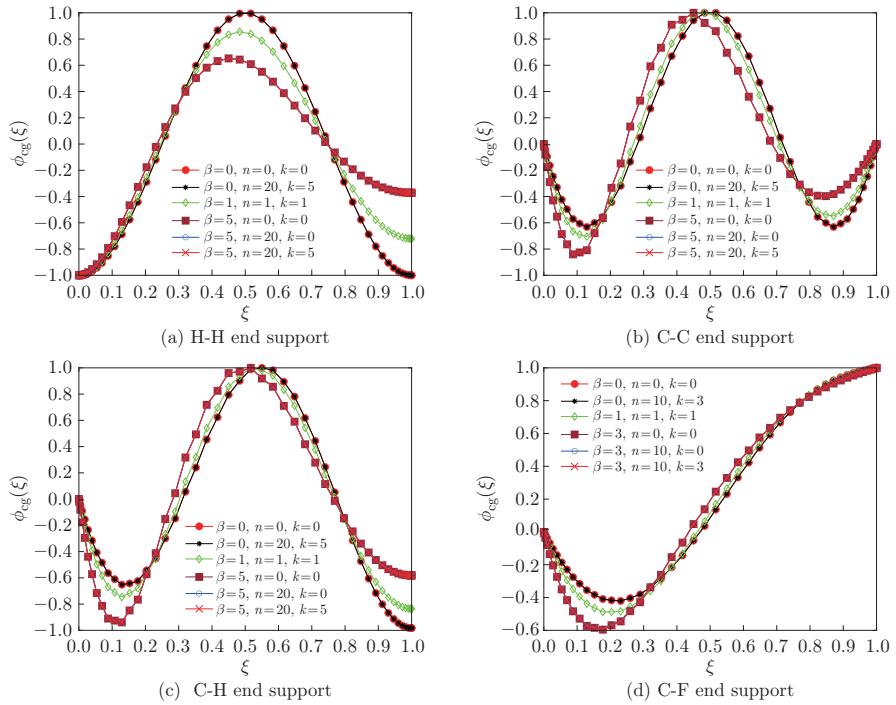

(a) H-H end support (b) C-C end support

(c) C-H end support (d) C-F end support

Fig. 9 Effects of the axial, radial, and circumferential FGM indexes on the second mode of the 3D FGM Timoshenko tube (rotation angle) under different types of boundary conditions ($L/R_o = 20$) (color online)

5 Conclusions

In this study, we introduce 3D FGM to construct the Timoshenko tube for resisting 3D directional loads. The natural dynamic characteristics of the novel tube with general end supports are comprehensively investigated. Considering the interactions among the longitudinal, transverse, and rotation deformations and taking the advantage of Hamilton's principle, we establish a novel model for the tube with the aid of the Timoshenko beam theory. The DQM in association with the Ritz method is utilized to solve the governing equations with variable coefficients. Numerical simulations are conducted to reveal the effects of the FGM indexes and boundary conditions on the natural frequencies and mode shapes of the Timoshenko tube. The main conclusions are included as follows.

(I) The comparison of the dimensionless frequencies and mode shapes of the 3D FGM Timoshenko tube obtained by the DQM with those predicted by the Ritz method and FEM confirms the correctness of the present results.

(II) The natural frequencies of the 3D FGM Timoshenko tube have an ascending trend with respect to the radial FGM index under the C-C boundary condition but an opposite trend under the other boundary conditions. When the constraint stiffness grows from the C-F end supports to the C-C end supports, the natural frequencies caused by the index β vary gradually from downtrend to uptrend.

(III) The natural frequencies of the 3D FGM Timoshenko tube with various supported edges decrease when the radial and circumferential FGM indexes increase.

(IV) The increasing axial FGM index gives rise to the anti-symmetry of the first two mode shapes for the transverse deflection and rotation angle.

The results are expected to provide important guidelines for improving multi-directional FGM tubes to resist 3D load-bearing in engineering.

Acknowledgements The current study is funded by the Middle-aged Top-notch Talent and Innovative Team Support Programs of Anhui Polytechnic University of China.

References

[1] GUPTA, A. and TALHA, M. Recent development in modeling and analysis of functionally graded materials and structures. *Progress in Aerospace Sciences*, **79**, 1–14 (2015)

[2] SHAW, L. L. The crack driving force of functionally graded materials. *Journal of Materials Science Letters*, **17**, 65–67 (1998)

[3] MA, L. S. and LEE, D. W. Exact solutions for nonlinear static responses of a shear deformable FGM beam under an in-plane thermal loading. *European Journal of Mechanics-A/Solids*, **31**, 13–20 (2012)

[4] BANERJEE, J. R. and ANANTHAPUVIRAJAH, A. Free vibration of functionally graded beams and frameworks using the dynamic stiffness method. *Journal of Sound and Vibration*, **422**, 34–47 (2018)

[5] RAD, A. B. Thermo-elastic analysis of functionally graded circular plates resting on a gradient hybrid foundation. *Applied Mathematics and Computation*, **256**, 276–298 (2015)

[6] SHEN, H., PAÏDOUSSIS, M. P., WEN, J., YU, D., and WEN, X. The beam-mode stability of periodic functionally-graded-material shells conveying fluid. *Journal of Sound and Vibration*, **333**, 2735–2749 (2014)

[7] TANG, Y. and YANG, T. Post-buckling behavior and nonlinear vibration analysis of a fluid-conveying pipe composed of functionally graded material. *Composite Structures*, **185**, 393–400 (2018)

[8] ZHEN, Y., GONG, Y., and TANG, Y. Nonlinear vibration analysis of a supercritical fluid-conveying pipe made of functionally graded material with initial curvature. *Composite Structures*, **268**, 113980 (2021)

[9] JIANG, Q., ZHOU, Z., and YANG, F. The transient response of hollow electrostrictive cylinder subjected to the electrical shock. *Archive of Applied Mechanics*, **91**, 4039–4051 (2021)

[10] LI, Z. M. and LIU, T. A new displacement model for nonlinear vibration analysis of fluid-conveying anisotropic laminated tubular beams resting on elastic foundation. *European Journal of Mechanics-A/Solids*, **86**, 104172 (2021)

[11] KADOLI, R. and GANESAN, N. Buckling and free vibration analysis of functionally graded cylindrical shells subjected to a temperature-specified boundary condition. *Journal of Sound and Vibration*, **289**, 450–480 (2006)

[12] FU, Y., ZHONG, J., SHAO, X., and CHEN, Y. Thermal postbuckling analysis of functionally graded tubes based on a refined beam model. *International Journal of Mechanical Sciences*, **96**, 58–64 (2015)

[13] LU, L., SHE, G. L., and GUO, X. M. Size-dependent postbuckling analysis of graphene reinforced composite microtubes with geometrical imperfection. *International Journal of Mechanical Sciences*, **199**, 106428 (2021)

[14] LU, L., WANG, S., LI, M., and GUO, X. M. Free vibration and dynamic stability of functionally graded composite microtubes reinforced with graphene platelets. *Composite Structures*, **272**, 114231 (2021)

[15] GHATAGE, P. S., KAR, V. R., and SUDHAGAR, P. E. On the numerical modelling and analysis of multi-directional functionally graded composite structures: a review. *Composite Structures*, **236**, 111837 (2020)

[16] NEJAD, M. Z., HADI, A., OMIDVARI, A., and RASTGOO, A. Bending analysis of bi-directional functionally graded Euler-Bernoulli nano-beams using integral form of Eringen's non-local elasticity theory. *Structural Engineering and Mechanics*, **67**, 417–425 (2018)

[17] LAL, R. and AHLAWAT, N. Buckling and vibrations of two-directional functionally graded circular plates subjected to hydrostatic in-plane force. *Journal of Vibration and Control*, **23**, 2111–2127 (2017)

[18] LAL, R. and DANGI, C. Dynamic analysis of bi-directional functionally graded Timoshenko nanobeam on the basis of Eringen's nonlocal theory incorporating the surface effect. *Applied Mathematics and Computation*, **395**, 125857 (2021)

[19] TANG, Y., LV, X. F., and YANG, T. Z. Bi-directional functionally graded beams: asymmetric modes and nonlinear free vibration. *Composites Part B: Engineering*, **156**, 319–331 (2019)

[20] CHEN, X. C. and LI, Y. H. Size-dependent post-buckling behaviors of geometrically imperfect microbeams. *Mechanics Research Communications*, **88**, 25–33 (2018)

[21] TANG, Y. and DING, Q. Nonlinear vibration analysis of a bi-directional functionally graded beam under hygro-thermal loads. *Composite Structures*, **225**, 111076 (2019)

[22] TANG, Y., MA, Z. S., DING, Q., and WANG, T. Dynamic interaction between bi-directional functionally graded materials and magneto-electro-elastic fields: a nano-structure analysis. *Composite Structures*, **264**, 113746 (2021)

[23] TANG, Y., WANG, T., MA, Z. S., and YANG, T. Magneto-electro-elastic modelling and nonlinear vibration analysis of bi-directional functionally graded beams. *Nonlinear Dynamics*, **105**, 2195–2227 (2021)

[24] HADI, A., NEJAD, M. Z., and HOSSEINI, M. Vibrations of three-dimensionally graded nanobeams. *International Journal of Engineering Science*, **128**, 12–23 (2018)

[25] SHU, C. and CHEW, Y. T. On the equivalence of generalized differential quadrature and highest order finite difference scheme. *Computer Methods in Applied Mechanics and Engineering*, **155**, 249–260 (1998)